Many-body States Description of Single-molecule Electroluminescence Driven by Scanning Tunneling Microscope

Kuniyuki Miwa,[†,§] Hiroshi Imada,[†] Miyabi Imai-Imada,[†,‡] Kensuke Kimura,[†,‡] Michael Galperin,[*,¶] and Yousoo Kim[*,†]

†*Surface and Interface Science Laboratory, RIKEN, Wako, Saitama 351-0198, Japan*

‡*Department of Advanced Materials Science, Graduate School of Frontier Science, The University of Tokyo, Kashiwa, Chiba 277-8651, Japan.*

¶*Department of Chemistry and Biochemistry, University of California San Diego, La Jolla, California 92093, United States*

§*Present address: Department of Chemistry and Biochemistry, University of California San Diego, La Jolla, California 92093, United States*

E-mail: migalperin@ucsd.edu; ykim@riken.jp

Phone: +1 (858) 246 0511; +81 (48) 467 4073

Abstract

Electron transport and optical properties of a single molecule in contact with conductive materials have attracted considerable attention owing to their scientific importance and potential applications. With recent progresses of experimental techniques, especially by the virtue of scanning tunneling microscope (STM)-induced light emission, where the tunneling current of the STM is used as an atomic-scale source for induction of light emission from a single molecule, it becomes possible to investigate single-molecule properties at sub-nanometer spacial resolution. Despite extensive experimental studies, the microscopic mechanism of electronic excitation of a single molecule in STM-induced light emission is yet to be clarified. Here we present a formulation of single-molecule electroluminescence driven by electron transfer between a molecule and metal electrodes based on a many-body state representation of the molecule. The effects of intra-molecular Coulomb interaction on conductance and luminescence spectra are investigated using the nonequilibrium Hubbard Green's function technique combined with first-principles calculations. We compare simulation results with experimental data and find that the intra-molecular Coulomb interaction is crucial for reproducing recent experiments for a single phthalocyanine molecule. The developed theory provides a unified description of both electron-transport and optical properties of a single molecule in contact with metal electrodes driven out of equilibrium, and thereby it contributes to a microscopic understanding of optoelectronic conversion in single molecules on solid surfaces and in nanometer-scale junctions.

Keywords

Single molecule luminescence, exciton formation, scanning tunneling microscope-induced light emission, nonequilibrium Hubbard Green's function technique, time-dependent density functional theory (TDDFT), Vibronic interaction

Since the theoretical prediction of the possibility to use individual molecules as functional building blocks in electronic devices[1] and the first experimental realization of a single-molecule conductance junction,[2] the field of molecular electronics has experienced tremendous development. Molecular junctions are now widely used as both nanoscale devices and platforms for the study of fundamental physical properties of materials at nanometer scale.[3,4] Furthermore, recent progress in nanometer-scale fabrication techniques combined with optical technologies has allowed optical experiments on current-carrying molecular junctions.[5–17] These advances bring molecular electronics and optical spectroscopy together, leading to the emergence of molecular optoelectronics.[18,19]

In the optical response of current-carrying molecular junctions, the electrons participate in both conductance and optical scattering. Unified description of the two processes requires combination of theoretical tools from quantum transport and optical spectroscopy.[20,21] Note that majority of quantum-transport formulations utilize quasiparticle language, while optical spectroscopy traditionally employs molecular many-body states. This results in a variety of optoelectronic formulations. For example, quasiparticle language was employed in current-induced light emission,[22–28] light-induced current,[29–32] Raman scattering,[33–37] and multi-dimensional spectroscopy in junctions.[38,39] Many-body formulations are usually restricted to the Lindblad/Redfield quantum master equation (QME) level of theory.[40–44] The latter is not adequate for description of junctions where the energy of coupling between a molecule and at least one of metal electrodes is higher than the thermal energy, so that $\Gamma \gg k_B T$ (here Γ is electron escape rate, k_B is the Boltzmann constant, and T is temperature). Instead, one can use many-body flavor Green function approaches, such as pseudoparticle nonequilibrium Green functions (PP-NEGF)[45] and NEGF formulated via Hubbard operators (Hubbard NEGF).[46] In these methodologies, molecule-electrodes coupling is taken into account within proper diagrammatic perturbation series expansion. We note that many-body flavor Green function approaches are free from limitations of the standard QME schemes. One of the authors applied the PP-NEGF methodology to description of Raman scattering,[47] multi-

dimensional spectroscopy,[48] and strong plasmon-exciton coupling (polariton)[49] in junctions. The Hubbard NEGF, recently introduced by us, was shown to be superior relative to the PP-NEGF at low orders of diagrammatic expansion.[50] Here we utilize the Hubbard NEGF for description of transport and optical response in a single molecule junction.

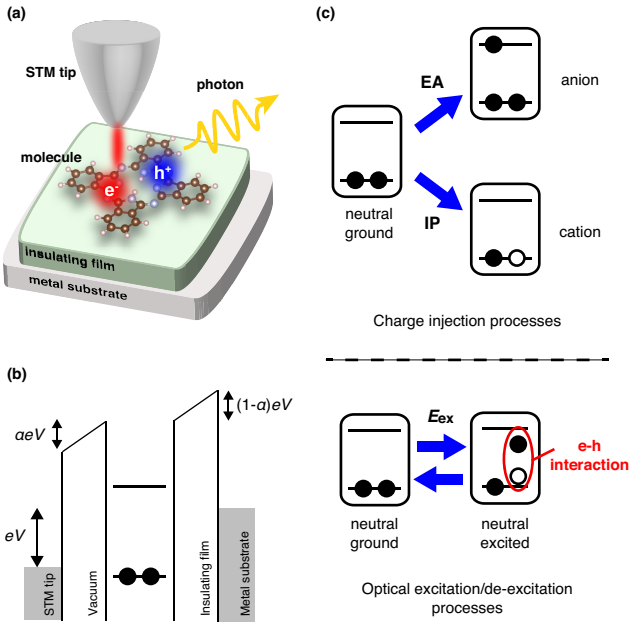

Figure 1: (a) Schematic picture of current-driven electroluminescence for a single phthalocyanine molecule adsorbed on a few atomic layers of insulator grown on a metal substrate. The tunneling current of a scanning tunneling microscope (STM) is used as an excitation source for induction of light emission from a sample. (b) Schematic energy diagram for a potential profile across a junction composed of the STM tip and a molecule adsorbed on an insulating film-covered metal surface with sample bias voltage V. Electrostatic potential drops both in the insulating film and in the vacuum region between the molecule and the metallic tip. (c) Schematic picture of electron attachment to and detachment from a neutral molecule (upper part), as well as optical excitation and de-excitation of the neutral molecule (lower part). Black and white dots represent an electron and a hole, respectively. Horizontal lines denote the energetic position of electron affinity (EA) and ionized potential (IP) for the molecule.

Experimental techniques involving a scanning tunneling microscope (STM) have been widely used to observe atomically resolved surface topography and to investigate the local density of states, thus providing information on the molecular electronic structure. The highly localized tunneling current of STM can also be used to induce light emission from a molecule, enabling the investigation of molecular optical properties at sub-molecular spa-

tial resolution in a well-defined manner [Figure 1(a)]. STM-induced light emission (STM-LE) spectroscopy has been applied to investigate molecular electroluminescence,[51–62] energy transfer between individual molecules,[63–65] and the interplay between the dielectric response of metals and intra-molecular electronic excitations.[24–26,66–68] For STM-LE from a single molecule, a few atomic layers of insulator have been used to partially decouple the molecular electronic structure from the electronic states of the underlying metal substrate.[69,70] In such a system, the differential conductance dI/dV spectra provide information on the electron affinity (EA) and ionization potential (IP) of the molecule adsorbed on the surface.[71] The energy difference between the IP and EA of a given system is commonly defined as the fundamental gap of the system.[72] The transport gap observed in the conductance measurement is slightly wider than the fundamental gap. This could primarily be attributed to a drop of the electrostatic potential both in the insulating film and in the vacuum region between the molecule and the metallic tip [Figure 1(b)]. In photo-emission processes of a single molecule, a key quantity is the optical gap, which differs from the fundamental gap by the exciton binding energy that is often substantial [Figure 1(c)]. Therefore, the difference between the measured transport and optical gaps is typically attributed to the exciton binding energy and the potential drop.

In previous studies on STM-LE from an individual phthalocyanine molecule adsorbed on an ultrathin NaCl film-covered Ag surface, Zhang *et al.* explained the difference between the observed transport and the optical gaps in terms of the potential drop, whereas the Coulomb interactions between electrons occupying molecular orbitals were neglected.[63] As the molecular electronic structure is partially decoupled from metal electronic states by the insulating film, the intra-molecular Coulomb interaction is expected to play an essential role in the electroluminescence process. For example, such interaction was shown to be significant for description of intra-molecular charge transfer processes in junctions.[73,74] However, its effect on the STM-LE processes have not yet been discussed. Many-body states are a convenient basis for such a study,[75–80] and taking into account that an adsorbed molecule

is not completely decoupled from the metal substrate ($\Gamma \gg k_B T$) theoretical treatment beyond Lindblad/Redfiled QME is required. In particular, such treatment allows us to account for broadened features resulting from the system-baths couplings (coupling with metal electrodes, radiation field, etc.) in the spectrum.

Here we apply the Hubbard NEGF method[46,50] to study effects of exciton binding energy on conductance and luminescence spectra. The importance of intra-molecular Coulomb interaction is emphasized in explaining experimental data for a single phthalocyanine molecule, and the microscopic mechanism for electronic excitation of the molecule in STM-LE processes is proposed. We note that while below molecular excitation is assumed to be caused by electron transfer between electrodes and molecule, an alternative mechanism due to energy transfer was also suggested in the literature.[65] While electron transfer, when it is energetically accessible, will probably be one of main contributions to electroluminescence, energy transfer may become dominant when electron transfer mechanism is blocked.

The paper is organized as follows. After the introduction of a molecular junction model, the simulation of the current and photon fluxes is discussed. Subsequently, first-principles calculations and comparison of the numerical results with the experimental data are presented. Based on the results, it is argued that the intra-molecular Coulomb interaction plays an important role in in the STM-LE experiments in Refs. 63,64,67. The paper is concluded by summarizing the findings and indicating directions for future research.

Model and Method. We consider a junction consisting of a molecule, M, coupled to two electrodes, tip and sub, and to continuum of empty radiation field modes, ph. Born-Oppenheimer (vibronic) states of the isolated molecule $|S\rangle \equiv |e_m\rangle\,|v_n^{(e_m)}\rangle$ are chosen as a basis in the molecular subspace. Here e_m denotes a particular state in electronic many-body states of the molecule, and $v_n^{(e_m)}$ indicates vibrational states for the electronic state $|e_m\rangle$. Electrons in the electrodes and photons of the radiation field are described within standard

second quantization. Hamiltonian of the junction is

$$\hat{H} = \hat{H}_{\rm M} + \sum_{B={\rm tip,sub,ph}} \Big(\hat{H}_B + \hat{V}_B \Big). \tag{1}$$

where H_M and H_B ($B = \mathrm{tip}, \mathrm{sub}, \mathrm{ph}$) are Hamiltonians of the molecule and baths (electrodes and radiation field). V_B describes coupling between the molecule M and the bath B. Explicit expressions are

$$\hat{H}_{\rm M} = \sum_{S\in M} E_S \hat{X}_{SS} \tag{2}$$

$$\hat{H}_K = \sum_{k\in K} \epsilon_k \hat{c}_k^\dagger \hat{c}_k \tag{3}$$

$$\hat{H}_{\rm ph} = \sum_{\alpha} \hbar\omega_\alpha \hat{a}_\alpha^\dagger \hat{a}_\alpha \tag{4}$$

$$\hat{V}_K = \sum_{\substack{k\in K \\ S_1,S_2\in M}} \Big(V_{(S_1S_2),k} \hat{X}_{S_1S_2}^\dagger \hat{c}_k + \mathrm{H.c.} \Big) \tag{5}$$

$$\hat{V}_{\rm ph} = \sum_{\substack{\alpha \\ S_1,S_2\in M}} \Big(U_{(S_1S_2),\alpha} \hat{X}_{S_1S_2}^\dagger \hat{a}_\alpha + \mathrm{H.c.} \Big). \tag{6}$$

Here, $K = \mathrm{tip}, \mathrm{sub}$ indicates electrodes (STM tip and metal substrate), and $\hat{X}_{S_1S_2} = |S_1\rangle\langle S_2|$ denotes the Hubbard (projection) operator, $\hat{c}_k^\dagger$ ($\hat{c}_k$) and $\hat{a}_\alpha^\dagger$ ($\hat{a}_\alpha$) create (annihilate) electron in state k of the electrodes and photon in mode α of the radiation field, respectively. $V_{(S_1S_2),k} = V_{(e_1e_2),k} \langle v_2^{(e_2)} | v_1^{(e_1)} \rangle$ is the electron transfer (ET) matrix element from the electrode state k into the molecule resulting in a transition between electronic states $|e_1\rangle \to |e_2\rangle$ ($|e_2\rangle$ has one electron more than $|e_1\rangle$); the transition is dressed with the Franck-Condon overlap integral $\langle v_2^{(e_2)} | v_1^{(e_1)} \rangle$. $U_{(S_1S_2),\alpha} = U_{(e_1e_2),\alpha} \langle v_2^{(e_2)} | v_1^{(e_1)} \rangle$ is the intra-molecular (optical) transition (OT) matrix element between electronic states $|e_1\rangle$ and $|e_2\rangle$ caused by absorption of a photon with frequency ω_α.

Electron flux I_K from the electrode K to the molecule M and photon flux $J_{\rm ph}$ from the molecule M into radiation field modes ph, are calculated from simple generalization of the

celebrated Meir-Wingreen expression.[81,82] Explicit expressions for the fluxes at steady-state are

$$I_K = \int_{-\infty}^{+\infty} \frac{d\omega}{2\pi}\, I_K(\omega) \equiv \int_{-\infty}^{+\infty} \frac{d\omega}{2\pi}\, \frac{e}{\hbar} \mathrm{Tr}_{\mathrm{ET}} \left[\sigma_K^{<}(\omega)\mathcal{G}^{>}(\omega) - \sigma_K^{>}(\omega)\mathcal{G}^{<}(\omega)\right], \tag{7}$$

$$J_{\mathrm{ph}} = \int_{-\infty}^{+\infty} \frac{d\omega}{2\pi}\, J_{\mathrm{ph}}(\omega) \equiv \int_{-\infty}^{+\infty} \frac{d\omega}{2\pi}\, \frac{1}{\hbar} \mathrm{Tr}_{\mathrm{OT}} \left[\sigma_{\mathrm{ph}}^{<}(\omega)\mathcal{G}^{>}(\omega) - \sigma_{\mathrm{ph}}^{>}(\omega)\mathcal{G}^{<}(\omega)\right]. \tag{8}$$

Here $\mathrm{Tr}_{\mathrm{ET}}[\ldots]$ and $\mathrm{Tr}_{\mathrm{OT}}[\ldots]$ indicates respectively trace over all electron and optical transfer transitions in M. $\sigma_K^{\lessgtr}$ and $\sigma_{\mathrm{ph}}^{\lessgtr}$ are lesser and greater projections of the electron self-energies due to coupling to the electrode K and the radiation field

$$[\sigma_K(\tau,\tau')]_{(S_1S_2),(S_3S_4)} \equiv \sum_{k\in K} V_{(S_1S_2),k}\, g_k(\tau,\tau')\, V_{k,(S_3S_4)} \tag{9}$$

$$[\sigma_{\mathrm{ph}}(\tau,\tau')]_{(S_1S_2),(S_3S_4)} \equiv \sum_{\alpha} U_{(S_1S_2),\alpha}\, f_\alpha(\tau,\tau')\, U_{\alpha,(S_3S_4)} \tag{10}$$

where $g_k(\tau,\tau') = -\frac{i}{\hbar}\langle T_c\, \hat{c}_k(\tau)\, \hat{c}_k^\dagger(\tau')\rangle$ and $f_\alpha(\tau,\tau') = -\frac{i}{\hbar}\langle T_c\, \hat{a}_\alpha(\tau)\, \hat{a}_\alpha^\dagger(\tau')\rangle$ are respectively Green functions for free electron in state k of the electrode K and free photon in mode α of the radiation field. τ and τ' are the Keldysh contour variables, and T_c is the contour ordering operator. $\mathcal{G}^{\lessgtr}$ in Eqs. (7)-(8) are lesser and greater projections of the molecular nonequilibrium Hubbard Green function

$$\mathcal{G}_{(S_1S_2)(S_3S_4)}(\tau,\tau') = -\frac{i}{\hbar}\langle T_c\, \hat{X}_{S_1S_2}(\tau)\, \hat{X}^\dagger_{S_3S_4}(\tau')\rangle. \tag{11}$$

Assuming timescale separation between dynamics of electron and vibrational molecular degrees of freedom and following Ref. 83 we introduce decoupling inherent in the Born-Oppenheimer approximation

$$\mathcal{G}_{(S_1S_2)(S_3S_4)}(\tau,\tau') \approx G_{(e_1e_2)(e_3e_4)}(\tau,\tau')\; K_{\left(v_1^{(e_1)}v_2^{(e_2)}\right)\left(v_3^{(e_3)}v_4^{(e_4)}\right)}(\tau,\tau') \tag{12}$$

where

$$G_{(e_1e_2)(e_3e_4)}(\tau,\tau') = -\frac{i}{\hbar}\left\langle T_c\,\hat{X}_{e_1e_2}(\tau)\,\hat{X}^{\dagger}_{e_3e_4}(\tau')\right\rangle \tag{13}$$

$$K_{\left(v_1^{(e_1)}v_2^{(e_2)}\right)\left(v_3^{(e_3)}v_4^{(e_4)}\right)}(\tau,\tau') = \left\langle T_c\,\hat{X}_{v_1^{(e_1)}v_2^{(e_2)}}(\tau)\,\hat{X}^{\dagger}_{v_3^{(e_3)}v_4^{(e_4)}}(\tau')\right\rangle \tag{14}$$

Dressing K with Franck-Condon overlap integrals yields generalized Franck-Condon factor

$$FC_{\left(v_1^{(e_1)}v_2^{(e_2)}\right)\left(v_3^{(e_3)}v_4^{(e_4)}\right)}(\tau,\tau') = \langle v_1^{(e_1)}|v_2^{(e_2)}\rangle\, K_{\left(v_1^{(e_1)}v_2^{(e_2)}\right)\left(v_3^{(e_3)}v_4^{(e_4)}\right)}(\tau,\tau')\,\langle v_4^{(e_4)}|v_3^{(e_3)}\rangle \tag{15}$$

Below we disregard effect of electron dynamics on the Frank-Condon factors FC. This simplifies expression (12) by reducing consideration to diagonal molecular transfers only (i.e. $e_1 = e_3$, $e_2 = e_4$, $v_1^{(e_1)} = v_3^{(e_3)}$, $v_2^{(e_2)} = v_4^{(e_4)}$). Franck-Condon factors are evaluated under assumption of equilibrium population of vibrational degrees of freedom. Evaluation of the electron Green functions G employs second order diagrammatic technique for the Hubbard Green functions (see Ref. 46 for details).

Hubbard NEGF simulations. Using many-body state representation of the molecule, the information of the molecular electronic and vibrational structure obtained by first-principles calculations can be conveniently incorporated into simulations of the electron transport and the optical properties of molecular junctions.[47,84] Molecular many-body states (ground and excited electronic states in different charging blocks, vibronic molecular states, etc.) calculated by quantum chemistry methods for the equilibrium isolated molecule are utilized in the Hubbard-NEGF calculations as a basis for description of transport and optical response of the molecular junction.

Here, the Hubbard NEGF method introduced above is used in theoretical modeling of STM-LE experiment for a single metal-free phthalocyanine (H_2Pc) molecule [Figure 2(a)] adsorbed on three monolayers of NaCl grown on an Ag(111) surface. Qualitative analysis of the effects of the electrostatic potential profile across the junction and the intra-molecular Coulomb interaction on the system response is presented in the Supporting information,

Section 1. It indicates that the latter plays an important role in reproducing conductance and luminescence spectra observed in the experiments. Numerical study based on the Hubbard NEGF simulations combined with first-principles calculations confirms conclusions of the qualitative analysis.

The parameters for the electronic and vibrational structure of the isolated molecule were obtained by first-principles calculations based on the density functional theory (DFT) and time-dependent DFT (TDDFT) implemented in the Gaussian 16.[85] In our analysis we consider the ground, first excited, and second excited electronic states with singlet spin state of the neutral molecule, first and second excited electronic states with triplet spin state of the neutral molecule, ground electronic state with doublet spin state of the cation, and ground and first excited electronic states with doublet spin state of the anion. The optimized geometry and the vibrational modes for each electronic state were calculated to obtain the overlap integral $\langle v_1^{(e_1)}|v_2^{(e_2)}\rangle$ by the method implemented in the Gaussian 16.[86–89] Range-separate hybrid density functional (LC-wHPBE)[90] with system-specific range separation parameter[91] was utilized in the simulations. The electronic wave functions were expanded using the triple-zeta valence basis augmented with diffuse functions (AUG-cc-pVTZ) on all atoms.[92] The detailed information on the DFT/TDDFT calculations is given in the Supporting Information, Section 2.

Other necessary parameters were chosen to be representative of a realistic experimental situation. The image interaction energy for a molecule adsorbed on a dielectric film grown on a metal substrate has been investigated based on the DFT calculation results and on the analysis using the dielectric model introduced in Ref. 93. The shift of the fundamental gap for the adsorbed molecule from its value for a molecule in the gas phase was estimated as 1.62 eV based on Eq. (6) in Ref. 93, with the parameters for H_2Pc adsorbed on a trilayer NaCl film supported by a metal substrate. Taking the dielectric constant of ultrathin NaCl film as 5.62 (using the value for bulk NaCl as a reference), the effective thickness of the film as 9.21 Å, and the tip-film distance as 10.07 Å, the value of the parameter characterizing

potential profile across the junction, α, was obtained to be 0.86. Using the result of the DFT calculation for 3ML-NaCl/Ag(100) in Ref. 94 as a reference, the work function for 3ML-NaCl/Ag(111) was set to 3.53 eV. The temperature is set as 5 K. The coupling strength between the molecule and electrode K (tip or sub) is characterized by electron escape rate, $\Gamma^K_{(S_1S_2),(S_3S_4)}(E) = 2\pi \sum_{k\in K} V_{(S_1S_2),k} V_{k,(S_3S_4)} \delta(E - \epsilon_k)$, is assumed to be energy independent (the wide-band approximation) and for all electronic transitions set as 2.5 meV. Further details regarding the parameter setting are given in Supporting Information, Section 3.

For the sake of simplicity, the Hubbard I approximation[46] was employed, and the diagonal elements of self-energy were used to compute the diagonal elements G_{mm} of the Hubbard Green's functions. The obtained Hubbard Green's functions were used in Eqs. (7) and (8) to calculate current I_K and photon flux J_{ph} in the junction. In simulation of the latter we follow Refs. 64,67, where transition from the first excited to the ground singlet spin state of the neutral molecule was reported as dominant contribution to the observed luminescence.

To verify the proposed theory, the computational results were compared with the experimental data. The experimental measurements were performed using an STM (Omicron) operated under ultra-high vacuum (5.0×10^{-11} Torr) at a temperature of 4.7 K. A (111)-terminated Ag single crystal was used as a metallic substrate for growing a trilayer NaCl film. H_2Pcs were deposited onto the NaCl film-covered Ag(111) surface and observed with an Ag tip. The details regarding the experimental setup are presented in Supporting Information, Section 4.

The experimental and computational results for the dI/dV spectra are shown in Figure 2(b). The experimental results exhibit two peaks, one for negative bias voltage near -2.30 V and the other for positive bias voltage near $+0.55$ V. This indicates that the transport gap of this system is 2.85 eV. The computational results for the dI/dV spectra exhibit peaks for both positive and negative bias voltage. The peak appears near -2.30 V, which corresponds to the many-body state transition between ground electronic state of the cation and the neutral molecule [top panel of Figure 2(c)]. The low intensity peak appears near

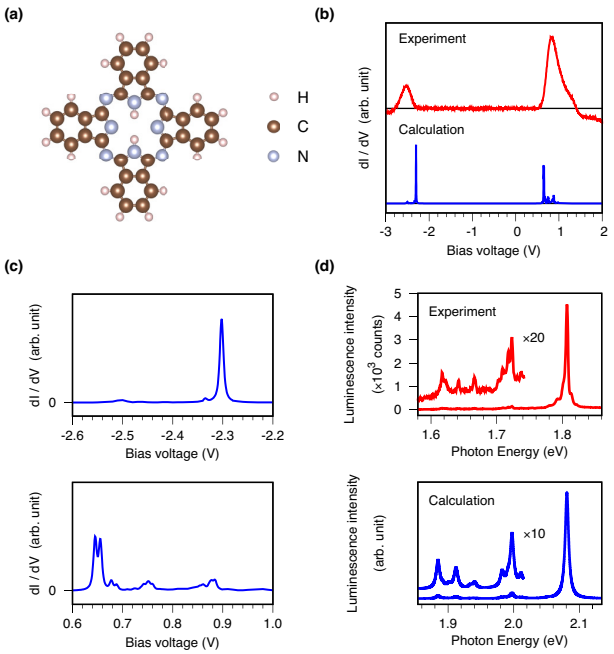

Figure 2: (a) Molecular structure of metal-free phthalocyanine (H_2Pc). Pink, brown, and blue spheres represent hydrogen, carbon, and nitrogen atoms, respectively. (b) Differential conductance dI/dV spectra. Red and blue lines represent experimental and computational results, respectively. Experimental data were obtained by constant-current dI/dV measurement using a bias voltage $V = 2.4$ V and a tunneling current $I = 3$ pA as a set point. (c) Numerical calculation results of dI/dV spectra for the ranges -2.6 V $< V < -2.2$ V (top panel) and 0.6 V $< V <$ 1.0 V (bottom panel). (d) Luminescence spectra obtained by STM-LE measurement (red line) and numerical calculation result of $J_{\rm ph}$ (blue line). The measurement conditions were $V = -2.5$ V, $I = 30$ pA, and exposure time $t = 60$ s.

-2.34 V and -2.50 V, corresponding to the many-body state transitions accompanied by vibrational excitations. For the positive bias voltage, as shown in the bottom panel of Figure 2(c), peaks appear near 0.645 and 0.655 V. The peak near 0.645 V is attributed to the many-body state transition between the ground electronic state of the anion and the neutral molecule. The peak near 0.655 V is attributed to the many-body state transition between the ground electronic state of the neutral molecule and the first excited electronic state of the anion. The low intensity peaks in the range $V > 0.68$ V correspond to the many-body state transitions associated with vibrational excitations.

The width of the calculated conductance peaks is considerably narrower than that of experimentally measured peaks. It is noteworthy that even though the coupling of the electron

with the molecular vibrational quantum (vibron) was taken into account, the coupling of the electron with the substrate phonon was not considered in this study. Repp *et al.* reported that broad line shapes observed for a single, localized electronic state induced by Cl vacancies in ultrathin NaCl film supported by a metal substrate were caused by strong electron-phonon coupling.[95] The dependence of peak width in the dI/dV spectra for a molecule on various types of insulating films, such as NaCl, RbI, and Xe films, was considered in Refs. 96,97. Qualitative analysis of the effects of electron–phonon coupling on the spectral profile is given in the Supporting Information, Section 5. Hence, the quantitative analysis of the electron–phonon coupling and the inclusion of this coupling in the theoretical method developed in this study are expected to reproduce the peak width in the dI/dV spectra. However, as the transport gap was well reproduced in the present calculation and the experimental system is too complicated to rigorously conduct a quantitative analysis of electron–phonon coupling, the analysis presented here proceeds without considering the details regarding the effects of electron–phonon coupling.

Measured and calculated luminescence spectra are shown in Figure 2(d). The experimental results show a high-intensity peak near 1.81 eV and several low-intensity peaks in the energy range lower than 1.81 eV. The optical gap of this system is estimated as 1.81 eV, and the low-intensity peaks are attributed to the radiative decay of the molecular exciton accompanied by vibrational excitations. The computational results show a high-intensity peak at 2.08 eV. As the TDDFT with Tamm–Dancoff approximation, which was used in this study, overestimates the singlet excitation energy, the calculated optical gap of the molecule is wider than the measured optical gap by approximately 0.27 eV, whereas vibrational side peaks observed in the experiment are well reproduced in the computational results.

Discussion. Based on the results, the excitation mechanism for the molecule in the STM-LE process is proposed as follows. For the bias voltage -2.30 V$< V < 0$ V, the molecular electronic state is in the ground electronic state with singlet spin state of the neutral molecule $|N, S_0\rangle$. For $V = -2.30$ V, an electron cannot hop from the metal substrate

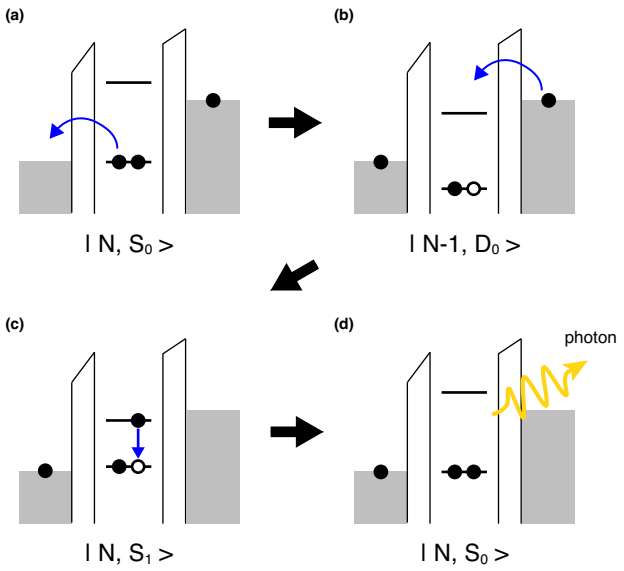

Figure 3: Schematics of the excitation mechanism for a single molecule in the STM-induced light emission process. Molecular electronic states are indicated as $|N_m, S_m\rangle$, where N_m and S_m denote the number of electrons in the molecule and the electronic state of the molecule, respectively. Excitation mechanism considered in the paper consists of set of electron transfer transitions as follows: (a) ground state of neutral molecule $|N, S_0\rangle$ to (b) the ground electronic state with doublet spin state of the cation $|N-1, D_0\rangle$ to (c) the first excited electronic state with singlet spin state of the neutral molecule $|N, S_1\rangle$ and (d) back to the ground state of neutral molecule $|N, S_0\rangle$ with emission of photon. Horizontal lines represent ionized potential (IP) and electron affinity (EA) for each electronic state. Black and white dots denote electron and hole, respectively.

to the neural molecule due to the Coulomb blockade; however, an electron transfer from the neutral molecule to the STM tip can occur [Figure 3(a)]. When the ground electronic state with doublet spin state of the cation $|N-1, D_0\rangle$ is realized, an electron can hop from the metal substrate to the molecule [Figure 3(b)]. This realizes the ground or excited electronic state of the neutral molecule, with the latter implying the formation of an electron–hole pair (exciton) in the molecule [Figure 3(c)]. Upon the radiative decay of a molecular exciton accompanying the many-body state transition from the first excited electronic state with singlet spin state of the neutral molecule $|N, S_1\rangle$ to $|N, S_0\rangle$, the energy is emitted to the radiation field [Figure 3(d)]. The proposed mechanism is verified by comparison with the experiments as follows.

Figure 4 shows the computational and experimental results for the dependence of lumi-

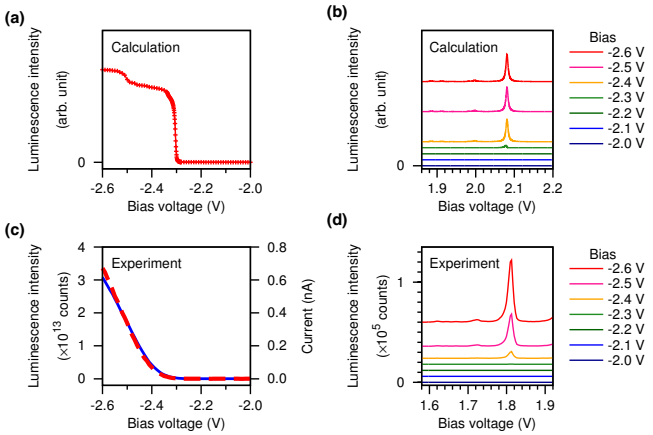

Figure 4: Computational and experimental results for the dependence of molecule luminescence on the bias voltage. (a) Computational results for the integrated luminescence intensity $J_{\rm ph}^{\rm total} = \int d\omega J_{\rm ph}(\omega)$ as a function of the applied bias voltage V. (b) Computational results for the luminescence spectra $J_{\rm ph}$ at the various bias voltages. Red, dark-pink, yellow, green, dark-green, blue, and dark-blue lines are $J_{\rm ph}$ at $V = -2.6$, -2.5, -2.4, -2.3, -2.2, -2.1, and -2.0 V, respectively. (c) Experimental results for the dependence of luminescence intensity (red dashed line) and tunnel current (blue solid line) on the sample bias voltage. The tip-sample distance was fixed during the measurements (constant height mode). The data was obtained by changing the bias voltage by 10 meV, and a charge-coupled-device (CCD) photon detector was exposed for 1 s to acquire the luminescence spectra at each bias voltage. Luminescence intensities were calculated by adding up the photons detected in the wavelength range 680 nm to 700 nm (in the energy range 1.771 eV to 1.823 eV). (d) Experimental result for the bias voltage dependence of the luminescence spectra. The data was acquired in the constant height mode shown in (c). Red, dark-pink, yellow, green, dark-green, blue, and dark-blue lines correspond to the results at $V = -2.6$, -2.5, -2.4, -2.3, -2.2, -2.1, and -2.0 V, respectively.

nescence intensity on the bias voltage. In Figure 4(a), the computational results demonstrate that as the bias voltage V decreases, the integrated luminescence intensity $J_{\rm ph}^{\rm total} = \int d\omega J_{\rm ph}(\omega)$ significantly increases near $V = -2.30$ V and gradually increases for $V < -2.30$ V. The voltage at which the steps appear in the $J_{\rm ph}^{\rm total} - V$ curve corresponds to the peak position in the dI/dV spectra [upper panel of Figure 2(c)], indicating that the extraction of an electron from the molecule triggers the electronic excitation of the molecule. The gradual increase in $J_{\rm ph}^{\rm total}$ for $V < -2.3$ V is attributed to the increase in the vibrational states that are involved in the electron transfer between the molecule and the metals. That is, as V decreases, many-body state transitions accompanied by the vibrational excitations con-

tribute to the electron transfer between the molecule and the metals, leading to the increase in the tunneling current I and luminescence intensity $J_{\rm ph}^{\rm total}$. In Figures 4(c) and (d), the experimental results exhibit a significant increase in luminescence intensity near $V = -2.30$ V. The results indicate that the electron transfer between the molecule and the metals significantly contribute to the electronic excitation that leads to the molecular luminescence for $V \leq -2.30$ V. It is noteworthy that relatively weak luminescence was previously observed even for -2.30 V $< V < -1.81$ V .[62,64,65] Doppagne *et al.* suggested that the molecule could be excited by an energy transfer from electrons tunneling between the tip and the metal substrate.[62] Energy transfer from tunneling electrons[62,65] and/or from interface plasmons localized near the tip-sample gap region[24–26,41,42,66] to the molecule would lead to electronic excitation of the molecule even for the bias voltage -2.30 V $< V < -1.81$ V. However, as the luminescence intensity for -2.30 V $< V < -1.81$ V is significantly weaker than for $V \leq -2.30$ V, we assume that another mechanism (electron transfer between the molecule and the metals) may be an additional important contribution for $V \leq -2.30$ V. We reiterate that electron transfer is clearly not the only possible mechanism, and molecular excitation is possible also by energy transfer as was proposed in Ref. 65. This latter mechanism was not considered in our treatment. At the same time, it is probably safe to state that for any excitation mechanism the intra-molecular Coulomb interaction is a key factor in explaining the experimentally observed difference between the transport and optical gaps.

In conclusion, a nonequilibrium atomic limit formulation of current-driven single molecule electroluminescence was presented. This framework allows the description of a nonequilibrium open system consisting of a single molecule positioned between two metal electrodes in terms of many-body states of the isolated molecule, as well as the exact handling of the intra-molecular Coulomb interaction. The effect of exciton binding energy on conductance and luminescence spectra of the system was discussed by comparison with the experimental results for STM-LE from a single phthalocyanine molecule. Even though the difference between the transport and the optical gap observed in the experiment has been attributed

to the potential profile across the junction,[63] it was demonstrated that the intra-molecular Coulomb interaction plays a decisive role in reproducing the experimental results as well as in explaining this difference. Furthermore, the developed methodology was applied to a realistic experimental situation, where a metal-free phthalocyanine molecule was adsorbed on a NaCl film-covered Ag(111) surface. Based on the results, the mechanism for the electronic excitation of a single molecule in current-driven electroluminescence was proposed in terms of molecular many-body states. The results provide a fundamental understanding of current-driven electroluminescence processes and would aid in obtaining the true nature of electron/exciton dynamics underlying the optoelectronic conversion in a single molecule. They also provide a potential guideline to design single-molecule optoelectronic devices form the viewpoint of the energy level alignment of molecular electronic states with the metallic Fermi level, which is crucial for improving the efficiency of molecular electroluminescence. Thus, the findings in this study are expected to be of importance in the analysis of electron dynamics in single-molecule junctions driven out of equilibrium, in interpreting the results of single-molecule optical spectroscopy, and in designing single-molecule optoelectronic devices.

Acknowledgement

The authors thank John Weare, Eric Bylaska, and Glen Junior for fruitful discussions. This material is based upon work supported by the National Science Foundation under CHE-1565939, by the US Department of Energy under DE-SC0018201, and by the JSPS KAKENHI Grant Number 15H02025, 15J03915, 16K21623, 17H04796, 17H05470, 17K18766, 18H05257, 18J11856. Some of the numerical calculations were performed using the HOKUSAI supercomputer system at RIKEN.

Supporting Information Available

Supporting Information is available free of charge on the ACS Publication website.

It presents qualitative analysis for STM-LE from single ZnPc and H_2Pc molecules, gives technical details of the first-principles calculations, discusses parameter setting for image interaction and potential drop in the NaCl film, provides information about experimental setup, and shows effects of electron–phonon coupling on the spectral profile (PDF)

References

(1) Aviram, A.; Ratner, M. A. Molecular rectifiers. *Chemical Physics Letters* **1974**, *29*, 277–283.

(2) Reed, M. A.; Zhou, C.; Muller, C. J.; Burgin, T. P.; Tour, J. M. Conductance of a Molecular Junction. *Science* **1997**, *278*, 252–254.

(3) Aradhya, S. V.; Venkataraman, L. Single-molecule junctions beyond electronic transport. *Nature Nanotechnology* **2013**, *8*, 399–410.

(4) van der Molen, S. J. Toggled with electrical current. *Nature Nanotechnology* **2013**, *8*, 622–623.

(5) Ioffe, Z.; Shamai, T.; Ophir, A.; Noy, G.; Yutsis, I.; Kfir, K.; Cheshnovsky, O.; Selzer, Y. Detection of heating in current-carrying molecular junctions by Raman scattering. *Nature Nanotechnology* **2008**, *3*, 727–732.

(6) Ward, D. R.; Corley, D. a.; Tour, J. M.; Natelson, D. Vibrational and electronic heating in nanoscale junctions. *Nature Nanotechnology* **2010**, *6*, 33–38.

(7) Arielly, R.; Ofarim, A.; Noy, G.; Selzer, Y. Accurate Determination of Plasmonic Fields in Molecular Junctions by Current Rectification at Optical Frequencies. *Nano Letters* **2011**, *11*, 2968–2972.

(8) Shamai, T.; Selzer, Y. Spectroscopy of molecular junctions. *Chemical Society Reviews* **2011**, *40*, 2293.

(9) Zhang, R.; Zhang, Y.; Dong, Z. C.; Jiang, S.; Zhang, C.; Chen, L. G.; Zhang, L.; Liao, Y.; Aizpurua, J.; Luo, Y.; Yang, J. L.; Hou, J. G. Chemical mapping of a single molecule by plasmon-enhanced Raman scattering. *Nature* **2013**, *498*, 82–86.

(10) Yampolsky, S.; Fishman, D. A.; Dey, S.; Hulkko, E.; Banik, M.; Potma, E. O.; Apkarian, V. A. Seeing a single molecule vibrate through time-resolved coherent anti-Stokes Raman scattering. *Nature Photonics* **2014**, *8*, 650–656.

(11) Nakamura, M.; Yoshida, S.; Katayama, T.; Taninaka, A.; Mera, Y.; Okada, S.; Takeuchi, O.; Shigekawa, H. Mechanically activated switching of Si-based single-molecule junction as imaged with three-dimensional dynamic probe. *Nature Communications* **2015**, *6*, 8465.

(12) Crampton, K. T.; Zeytunyan, A.; Fast, A. S.; Ladani, F. T.; Alfonso-Garcia, A.; Banik, M.; Yampolsky, S.; Fishman, D. A.; Potma, E. O.; Apkarian, V. A. Ultrafast Coherent Raman Scattering at Plasmonic Nanojunctions. *The Journal of Physical Chemistry C* **2016**, *120*, 20943–20953.

(13) Cocker, T. L.; Peller, D.; Yu, P.; Repp, J.; Huber, R. Tracking the ultrafast motion of a single molecule by femtosecond orbital imaging. *Nature* **2016**, *539*, 263–267.

(14) López-Martínez, M.; Artés, J. M.; Sarasso, V.; Carminati, M.; Díez-Pérez, I.; Sanz, F.; Gorostiza, P. Differential Electrochemical Conductance Imaging at the Nanoscale. *Small* **2017**, *13*, 1700958.

(15) Tallarida, N.; Lee, J.; Apkarian, V. A. Tip-Enhanced Raman Spectromicroscopy on the Angstrom Scale: Bare and CO-Terminated Ag Tips. *ACS Nano* **2017**, *11*, 11393–11401.

(16) Li, S.; Chen, S.; Li, J.; Wu, R.; Ho, W. Joint Space-Time Coherent Vibration Driven Conformational Transitions in a Single Molecule. *Physical Review Letters* **2017**, *119*, 176002.

(17) Yu, A.; Li, S.; Wang, H.; Chen, S.; Wu, R.; Ho, W. Visualization of Nanoplasmonic Coupling to Molecular Orbital in Light Emission Induced by Tunneling Electrons. *Nano Letters* **2018**, *18*, 3076–3080.

(18) Galperin, M.; Nitzan, A. Molecular optoelectronics: the interaction of molecular conduction junctions with light. *Physical Chemistry Chemical Physics* **2012**, *14*, 9421.

(19) Galperin, M. Photonics and spectroscopy in nanojunctions: a theoretical insight. *Chemical Society Reviews* **2017**, *46*, 4000–4019.

(20) Kadanoff, L. P.; Baym, G. *Quantum Statistical Mechanics*; W. A. Benjamin, Inc.: New York, 1962.

(21) Mukamel, S. *Principles of Nonlinear Optical Spectroscopy*; Oxford University Press: New York, 1995; p 576.

(22) Galperin, M.; Nitzan, A. Optical properties of current carrying molecular wires. *The Journal of Chemical Physics* **2006**, *124*, 234709.

(23) Harbola, U.; Maddox, J. B.; Mukamel, S. Many-body theory of current-induced fluorescence in molecular junctions. *Physical Review B* **2006**, *73*, 075211.

(24) Miwa, K.; Sakaue, M.; Kasai, H. Effects of interference between energy absorption processes of molecule and surface plasmons on light emission induced by scanning tunneling microscopy. *Journal of the Physical Society of Japan* **2013**, *82*, 123707.

(25) Miwa, K.; Sakaue, M.; Kasai, H. Interplay between plasmon luminescence and vibrationally resolved molecular luminescence induced by scanning tunneling microscopy. *Journal of the Physical Society of Japan* **2013**, *82*, 063715.

(26) Miwa, K.; Sakaue, M.; Gumhalter, B.; Kasai, H. Effects of plasmon energetics on light emission induced by scanning tunneling microscopy. *Journal of Physics: Condensed Matter* **2014**, *26*, 222001.

(27) Goswami, H. P.; Hua, W.; Zhang, Y.; Mukamel, S.; Harbola, U. Electroluminescence in Molecular Junctions: A Diagrammatic Approach. *Journal of Chemical Theory and Computation* **2015**, *11*, 4304–4315.

(28) Kaasbjerg, K.; Nitzan, A. Theory of Light Emission from Quantum Noise in Plasmonic Contacts: Above-Threshold Emission from Higher-Order Electron-Plasmon Scattering. *Phys. Rev. Lett.* **2015**, *114*, 126803.

(29) Galperin, M.; Nitzan, A. Current-Induced Light Emission and Light-Induced Current in Molecular-Tunneling Junctions. *Physical Review Letters* **2005**, *95*, 206802.

(30) Fainberg, B. D.; Jouravlev, M.; Nitzan, A. Light-induced current in molecular tunneling junctions excited with intense shaped pulses. *Physical Review B* **2007**, *76*, 245329.

(31) Hu, Z.; Ratner, M. A.; Seideman, T. Modeling light-induced charge transfer dynamics across a metal-molecule-metal junction: Bridging classical electrodynamics and quantum dynamics. *The Journal of Chemical Physics* **2014**, *141*, 224104.

(32) Ochoa, M. A.; Selzer, Y.; Peskin, U.; Galperin, M. Pump-Probe Noise Spectroscopy of Molecular Junctions. *JPCL* **2015**, *6*, 470–476.

(33) Galperin, M.; Ratner, M. A.; Nitzan, A. Raman scattering in current-carrying molecular junctions. *Journal of Chemical Physics* **2009**, *130*, 144109.

(34) Galperin, M.; Nitzan, A. Raman scattering from biased molecular conduction junctions: The electronic background and its temperature. *Physical Review B* **2011**, *84*, 195325.

(35) Banik, M.; Apkarian, V. A.; Park, T.-H.; Galperin, M. Raman Staircase in Charge Transfer SERS at the Junction of Fusing Nanospheres. *JPCL* **2013**, *4*, 88–92.

(36) Li, Y.; Doak, P.; Kronik, L.; Neaton, J. B.; Natelson, D. Voltage tuning of vibrational mode energies in single-molecule junctions. *Proceedings of the National Academy of Sciences* **2014**, *111*, 1282–1287.

(37) Dey, S.; Banik, M.; Hulkko, E.; Rodriguez, K.; Apkarian, V. A.; Galperin, M.; Nitzan, A. Observation and analysis of Fano-like lineshapes in the Raman spectra of molecules adsorbed at metal interfaces. *Physical Review B* **2016**, *93*, 035411.

(38) Rahav, S.; Mukamel, S. Multidimensional optical spectroscopy of a single molecule in a current-carrying state. *The Journal of Chemical Physics* **2010**, *133*, 244106.

(39) Agarwalla, B. K.; Harbola, U.; Hua, W.; Zhang, Y.; Mukamel, S. Coherent (photon) vs incoherent (current) detection of multidimensional optical signals from single molecules in open junctions. *The Journal of Chemical Physics* **2015**, *142*, 212445.

(40) Seldenthuis, J. S.; van der Zant, H. S. J.; Ratner, M. A.; Thijssen, J. M. Electroluminescence spectra in weakly coupled single-molecule junctions. *Physical Review B* **2010**, *81*, 205430.

(41) Tian, G.; Luo, Y. Electroluminescence of molecules in a scanning tunneling microscope: Role of tunneling electrons and surface plasmons. *Physical Review B* **2011**, *84*, 205419.

(42) Tian, G.; Liu, J. C.; Luo, Y. Density-Matrix Approach for the Electroluminescence of Molecules in a Scanning Tunneling Microscope. *Physical Review Letters* **2011**, *106*, 177401.

(43) Harbola, U.; Agarwalla, B. K.; Mukamel, S. Frequency-domain stimulated and spontaneous light emission signals at molecular junctions. *The Journal of Chemical Physics* **2014**, *141*, 074107.

(44) Fu, B.; Mosquera, M. A.; Schatz, G. C.; Ratner, M. A.; Hsu, L.-Y. Photoinduced Anomalous Coulomb Blockade and the Role of Triplet States in Electron Transport through an Irradiated Molecular Transistor. *Nano Letters* **2018**, *18*, 5015–5023.

(45) Aoki, H.; Tsuji, N.; Eckstein, M.; Kollar, M.; Oka, T.; Werner, P. Nonequilibrium dynamical mean-field theory and its applications. *Rev. Mod. Phys.* **2014**, *86*, 779–837.

(46) Chen, F.; Ochoa, M. A.; Galperin, M. Nonequilibrium diagrammatic technique for Hubbard Green functions. *The Journal of Chemical Physics* **2017**, *146*, 092301.

(47) White, A. J.; Tretiak, S.; Galperin, M. Raman Scattering in Molecular Junctions: A Pseudoparticle Formulation. *Nano Letters* **2014**, *14*, 699–703.

(48) Gao, Y.; Galperin, M. Simulation of optical response functions in molecular junctions. *The Journal of Chemical Physics* **2016**, *144*, 244106.

(49) White, A. J.; Fainberg, B. D.; Galperin, M. Collective Plasmon-Molecule Excitations in Nanojunctions: Quantum Consideration. *JPCL* **2012**, *3*, 2738–2743.

(50) Miwa, K.; Chen, F.; Galperin, M. Towards Noise Simulation in Interacting Nonequilibrium Systems Strongly Coupled to Baths. *Scientific Reports* **2017**, *7*, 9735.

(51) Qiu, X. H.; Nazin, G. V.; Ho, W. Vibrationally resolved fluorescence excited with submolecular precision. *Science* **2003**, *299*, 542–546.

(52) Dong, Z. C.; Guo, X. L.; Trifonov, A. S.; Dorozhkin, P. S.; Miki, K.; Kimura, K.; Yokoyama, S.; Mashiko, S. Vibrationally Resolved Fluorescence from Organic Molecules near Metal Surfaces in a Scanning Tunneling Microscope. *Physical Review Letters* **2004**, *92*, 086801.

(53) Ćavar, E.; Blüm, M. C.; Pivetta, M.; Patthey, F.; Chergui, M.; Schneider, W. D. Fluorescence and Phosphorescence from Individual C60 Molecules Excited by Local Electron Tunneling. *Physical Review Letters* **2005**, *95*, 196102.

(54) Dong, Z. C.; Zhang, X. L.; Gao, H. Y.; Luo, Y.; Zhang, C.; Chen, L. G.; Zhang, R.; Tao, X.; Zhang, Y.; Yang, J. L.; Hou, J. G. Generation of molecular hot electroluminescence by resonant nanocavity plasmons. *Nature Photonics supplementary information* **2010**, *4*, 50–54.

(55) Chen, C.; Chu, P.; Bobisch, C. A.; Mills, D. L.; Ho, W. Viewing the Interior of a Single Molecule: Vibronically Resolved Photon Imaging at Submolecular Resolution. *Physical Review Letters* **2010**, *105*, 217402.

(56) Reecht, G.; Scheurer, F.; Speisser, V.; Dappe, Y. J.; Mathevet, F.; Schull, G. Electroluminescence of a Polythiophene Molecular Wire Suspended between a Metallic Surface and the Tip of a Scanning Tunneling Microscope. *Physical Review Letters* **2014**, *112*, 047403.

(57) Lee, J.; Perdue, S. M.; Rodriguez Perez, A.; Apkarian, V. A. Vibronic Motion with Joint AngstromFemtosecond Resolution Observed through Fano Progressions Recorded within One Molecule. *ACS Nano* **2014**, *8*, 54–63.

(58) Merino, P.; Große, C.; Rosławska, A.; Kuhnke, K.; Kern, K. Exciton dynamics of C60-based single-photon emitters explored by Hanbury BrownTwiss scanning tunnelling microscopy. *Nature Communications* **2015**, *6*, 8461.

(59) Zhang, L.; Yu, Y.-J.; Chen, L.-G.; Luo, Y.; Yang, B.; Kong, F.-F.; Chen, G.; Zhang, Y.; Zhang, Q.; Luo, Y.; Yang, J.-L.; Dong, Z.-C.; Hou, J. G. Electrically driven single-photon emission from an isolated single molecule. *Nature Communications* **2017**, *8*, 580.

(60) Merino, P.; Rosławska, A.; Große, C.; Leon, C. C.; Kuhnke, K.; Kern, K. Bimodal exciton-plasmon light sources controlled by local charge carrier injection. *Science Advances* **2018**, *4*, eaap8349.

(61) Rosławska, A.; Merino, P.; Große, C.; Leon, C. C.; Gunnarsson, O.; Etzkorn, M.; Kuhnke, K.; Kern, K. Single Charge and Exciton Dynamics Probed by Molecular-Scale-Induced Electroluminescence. *Nano Letters* **2018**, *18*, 4001–4007.

(62) Doppagne, B.; Chong, M. C.; Bulou, H.; Boeglin, A.; Scheurer, F.; Schull, G. Electrofluorochromism at the single-molecule level. *Science* **2018**, *361*, 251–255.

(63) Zhang, Y.; Luo, Y.; Zhang, Y.; Yu, Y.-J.; Kuang, Y.-M.; Zhang, L.; Meng, Q.-S.; Luo, Y.; Yang, J.-L.; Dong, Z.-C.; Hou, J. G. Visualizing coherent intermolecular dipoledipole coupling in real space. *Nature* **2016**, *531*, 623–627.

(64) Imada, H.; Miwa, K.; Imai-Imada, M.; Kawahara, S.; Kimura, K.; Kim, Y. Real-space investigation of energy transfer in heterogeneous molecular dimers. *Nature* **2016**, *538*, 364–367.

(65) Doppagne, B.; Chong, M. C.; Lorchat, E.; Berciaud, S.; Romeo, M.; Bulou, H.; Boeglin, A.; Scheurer, F.; Schull, G. Vibronic Spectroscopy with Submolecular Resolution from STM-Induced Electroluminescence. *Physical Review Letters* **2017**, *118*, 127401.

(66) Schneider, N. L.; Berndt, R. Plasmonic exciation of light emission and absorption by porphyrine molecules in a scanning tunneling microscope. *Physical Review B* **2012**, *86*, 035445.

(67) Imada, H.; Miwa, K.; Imai-Imada, M.; Kawahara, S.; Kimura, K.; Kim, Y. Single-Molecule Investigation of Energy Dynamics in a Coupled Plasmon-Exciton System. *Physical Review Letters* **2017**, *119*, 013901.

(68) Zhang, Y.; Meng, Q.-S.; Zhang, L.; Luo, Y.; Yu, Y.-J.; Yang, B.; Zhang, Y.; Esteban, R.; Aizpurua, J.; Luo, Y.; Yang, J.-L.; Dong, Z.-C.; Hou, J. G. Sub-nanometre control of the coherent interaction between a single molecule and a plasmonic nanocavity. *Nature Communications* **2017**, *8*, 15225.

(69) Rossel, F.; Pivetta, M.; Schneider, W. D. Luminescence Experiments on Supported Molecules with the Scanning Tunneling Microscope. *Surface Science Reports* **2010**, *65*, 129–144.

(70) Kuhnke, K.; Große, C.; Merino, P.; Kern, K. Atomic-Scale Imaging and Spectroscopy of Electroluminescence at Molecular Interfaces. *Chemical Reviews* **2017**, *117*, 5174–5222.

(71) Repp, J.; Meyer, G.; Stojković, S. M.; Gourdon, A.; Joachim, C. Molecules on Insulating Films: Scanning-Tunneling Microscopy Imaging of Individual Molecular Orbitals. *Physical Review Letters* **2005**, *94*, 026803.

(72) Refaely-Abramson, S.; Baer, R.; Kronik, L. Fundamental and excitation gaps in molecules of relevance for organic photovoltaics from an optimally tuned range-separated hybrid functional. *Physical Review B* **2011**, *84*, 075144.

(73) Baratz, A.; Galperin, M.; Baer, R. Gate-Induced Intramolecular Charge Transfer in a Tunnel Junction: A Nonequilibrium Analysis. *Journal of Physical Chemistry C* **2013**, *117*, 10257–10263.

(74) Baratz, A.; White, A. J.; Galperin, M.; Baer, R. Effects of electromagnetic coupling on conductance switching of a gated tunnel junction. *JPCL* **2014**, *5*, 3545–3550.

(75) Swart, I.; Sonnleitner, T.; Repp, J. Charge State Control of Molecules Reveals Modification of the Tunneling Barrier with Intramolecular Contrast. *Nano Letters* **2011**, *11*, 1580–1584.

(76) Schulz, F.; Ijas, M.; Drost, R.; Hamalainen, S. K.; Harju, A.; Seitsonen, A. P.; Liljeroth, P. Many-body transitions in a single molecule visualized by scanning tunnelling microscopy. *Nature Physics* **2015**, *11*, 229–234.

(77) Siegert, B.; Donarini, A.; Grifoni, M. Nonequilibrium spin crossover in copper phthalocyanine. *Physical Review B* **2016**, *93*, 121406.

(78) Yu, P.; Kocić, N.; Repp, J.; Siegert, B.; Donarini, A. Apparent Reversal of Molecular Orbitals Reveals Entanglement. *Physical Review Letters* **2017**, *119*, 056801.

(79) Schulz, F.; Ijäs, M.; Drost, R.; Hämäläinen, S. K.; Harju, A.; Seitsonen, A. P.; Liljeroth, P. Many-body transitions in a single molecule visualized by scanning tunnelling microscopy. *Nature Physics* **2015**, *11*, 229–234.

(80) Ervasti, M. M.; Schulz, F.; Liljeroth, P.; Harju, A. Single- and many-particle description of scanning tunneling spectroscopy. *Journal of Electron Spectroscopy and Related Phenomena* **2017**, *219*, 63–71.

(81) Haug, H.; Jauho, A.-P. *Quantum Kinetics in Transport and Optics of Semiconductors*, 2nd ed.; Springer, 2008; p 362.

(82) Gao, Y.; Galperin, M. Optical spectroscopy of molecular junctions: Nonequilibrium Greens functions perspective. *Journal of Chemical Physics* **2016**, *144*, 174113.

(83) Galperin, M.; Nitzan, A.; Ratner, M. A. Resonant inelastic tunneling in molecular junctions. *Physical Review B* **2006**, *73*, 045314.

(84) Yeganeh, S.; Ratner, M. a.; Galperin, M.; Nitzan, A. Transport in State Space: Voltage-Dependent Conductance Calculations of Benzene-1,4-dithiol. *Nano Letters* **2009**, *9*, 1770–1774.

(85) Frisch, M. J. et al. GAUSSIAN 16. 2016.

(86) Santoro, F.; Improta, R.; Lami, A.; Bloino, J.; Barone, V. Effective method to compute Franck-Condon integrals for optical spectra of large molecules in solution. *The Journal of Chemical Physics* **2007**, *126*, 084509.

(87) Santoro, F.; Lami, A.; Improta, R.; Barone, V. Effective method to compute vibrationally resolved optical spectra of large molecules at finite temperature in the gas phase and in solution. *The Journal of Chemical Physics* **2007**, *126*, 184102.

(88) Santoro, F.; Lami, A.; Improta, R.; Bloino, J.; Barone, V. Effective method for the computation of optical spectra of large molecules at finite temperature including the Duschinsky and HerzbergTeller effect: The Qx band of porphyrin as a case study. *The Journal of Chemical Physics* **2008**, *128*, 224311.

(89) Barone, V.; Bloino, J.; Biczysko, M.; Santoro, F. Fully Integrated Approach to Compute Vibrationally Resolved Optical Spectra: From Small Molecules to Macrosystems. *Journal of Chemical Theory and Computation* **2009**, *5*, 540–554.

(90) Henderson, T. M.; Izmaylov, A. F.; Scalmani, G.; Scuseria, G. E. Can short-range hybrids describe long-range-dependent properties? *The Journal of Chemical Physics* **2009**, *131*, 044108.

(91) Baer, R.; Livshits, E.; Salzner, U. Tuned Range-Separated Hybrids in Density Functional Theory. *Annual Review of Physical Chemistry* **2010**, *61*, 85–109.

(92) Dunning, T. H. Gaussian basis sets for use in correlated molecular calculations. I. The atoms boron through neon and hydrogen. *The Journal of Chemical Physics* **1989**, *90*, 1007–1023.

(93) Scivetti, I.; Persson, M. Frontier molecular orbitals of a single molecule adsorbed on thin insulating films supported by a metal substrate: electron and hole attachment energies. *Journal of Physics: Condensed Matter* **2017**, *29*, 355002.

(94) Prada, S.; Martinez, U.; Pacchioni, G. Work function changes induced by deposition of ultrathin dielectric films on metals: A theoretical analysis. *Physical Review B* **2008**, *78*, 235423.

(95) Repp, J.; Meyer, G.; Paavilainen, S.; Olsson, F.; Persson, M. Scanning Tunneling Spectroscopy of Cl Vacancies in NaCl Films: Strong Electron-Phonon Coupling in Double-Barrier Tunneling Junctions. *Physical Review Letters* **2005**, *95*, 225503.

(96) Liljeroth, P.; Repp, J.; Meyer, G. Current-Induced Hydrogen Tautomerization and Conductance Switching of Naphthalocyanine Molecules. *Science* **2007**, *317*, 1203–1206.

(97) Pavliček, N.; Swart, I.; Niedenführ, J.; Meyer, G.; Repp, J. Symmetry Dependence of Vibration-Assisted Tunneling. *Physical Review Letters* **2013**, *110*, 136101.

Graphical TOC Entry